Report

Ground Thermal Simulation and Probabilistic Pile Capacity Analysis in Permafrost

PCCH-Arctic report Nr.3

Author(s):

Yared Bekele, Anatoly O. Sinitsyn

Report No:

Client(s) (pos partner):

Research Council of Norway

SINTEF Community
Postal address:
Postboks 4760 Torgarden
7465 Trondheim

Switchboard: +47 40005100

info@sintef.no

Enterprise /VAT No:
NO 919 303 808 MVA

PCCH-Arctic Report Nr. 3

Ground Thermal Simulation and Probabilistic Pile Capacity Analysis in Permafrost

KEYWORDS
Climate change
Active layer thickness
Soil temperature
Axial pile capacity
Probabilistic analysis
Permafrost

VERSION
1.0

DATE
2025-05-01

AUTHOR(S)
Yared Bekele, Anatoly O. Sinitsyn

CLIENT(S)
Research Council of Norway

CLIENT'S REFERENCE
Agnes Aune

PROJECT NO.
102024652

NO. OF PAGES
33

SUMMARY
Detailed ground thermal simulations are performed for Longyearbyen, revealing significant shifts in active layer thickness and permafrost temperatures due to climate change, with the active layer projected to increase in thickness by 2070 and permafrost warming significantly. Ground thermal simulations provide a basis for these projections, highlighting potential impacts on infrastructure and ecosystems. A probabilistic methodology for evaluating pile foundation capacity in permafrost is introduced, employing Monte Carlo simulations to address uncertainties in environmental and material properties. Sensitivity analyses within this framework emphasize the importance of probabilistic approaches in geotechnical engineering, enabling more effective risk management and design optimization in response to changing permafrost conditions.

PREPARED BY
Yared Bekele

SIGNATURE

CHECKED BY
Stein Christensen

SIGNATURE

APPROVED BY
Sindre Log

SIGNATURE

REPORT NO.
2024:00121

ISBN
978-82-14-07186-3

CLASSIFICATION
Unrestricted

CLASSIFICATION THIS PAGE
Unrestricted

Document history

VERSION	DATE	VERSION DESCRIPTION
1.0	2025-05-01	First version of report.

Table of contents

APPENDICES

None

1 Introduction

In the ongoing efforts to protect and preserve cultural heritage, the PCCH-Arctic project has undertaken a comprehensive risk assessment to understand and mitigate the impacts of environmental changes on technical-industrial cultural heritage in Longyearbyen and Ny-Ålesund. A high-level risk assessment was previously performed, which laid the foundation for recognizing the threats posed to cultural heritage objects by different natural hazards; (Bekele, Y., Sinitsyn, A., 2023). Building on this work, the present report delves into a more nuanced and detailed risk analysis, focusing on the structural integrity of buildings and structures on heritage sites in the face of evolving ground conditions.

This report advances the discourse by conducting a lower-level risk assessment, offering a finer granularity of analysis than previously achieved. Central to this assessment are two main components: ground thermal simulation and the development of a probabilistic analysis methodology for evaluating the axial capacity of pile foundations—a critical aspect in the preservation of cultural heritage structures.

Ground thermal simulations form the cornerstone of this study, predicated on projected climate data that illuminate potential shifts in ground thermal regimes of permafrost due to climate change. By examining changes in the active layer thickness and permafrost temperature, this report provides a detailed insight into the potential risks posed to structure's foundations. The methodology and findings from these simulations are presented in detail in Chapter 3.

A probabilistic methodology has been developed to assess the axial capacity of a single pile. This approach not only enhances the understanding of current capacities but also anticipates future changes, thereby enabling proactive measures for cultural heritage conservation. The integration of results from ground thermal simulations into this methodology exemplifies a holistic approach to risk assessment, ensuring that the findings are both relevant and applicable to the real-world scenarios faced by cultural heritage sites. Chapter 4 presents this methodology and its findings. By combining thermal simulations results with probabilistic analysis, this report presents a methodology for risk assessment of the foundations of cultural heritage objects, offering valuable insights and methodologies that can be applied to safeguard technical-industrial cultural heritage against the backdrop of a changing climate.

2 Climate Data

2.1 Location

Climate data projection for the Longyearbyen area is obtained from the Norwegian Meteorological Institute. The projection is made on a 3 by 4 grid from the beginning of 1991 to the end of 2070. Figure 1 shows the location for the climate projection data on a map where the red dots indicate the center point of each grid cell in a 3 x 4 grid projection area. The variables included in the projection data are near-surface air temperature, surface temperature and ground temperature. This data is closely analysed in the following sections.

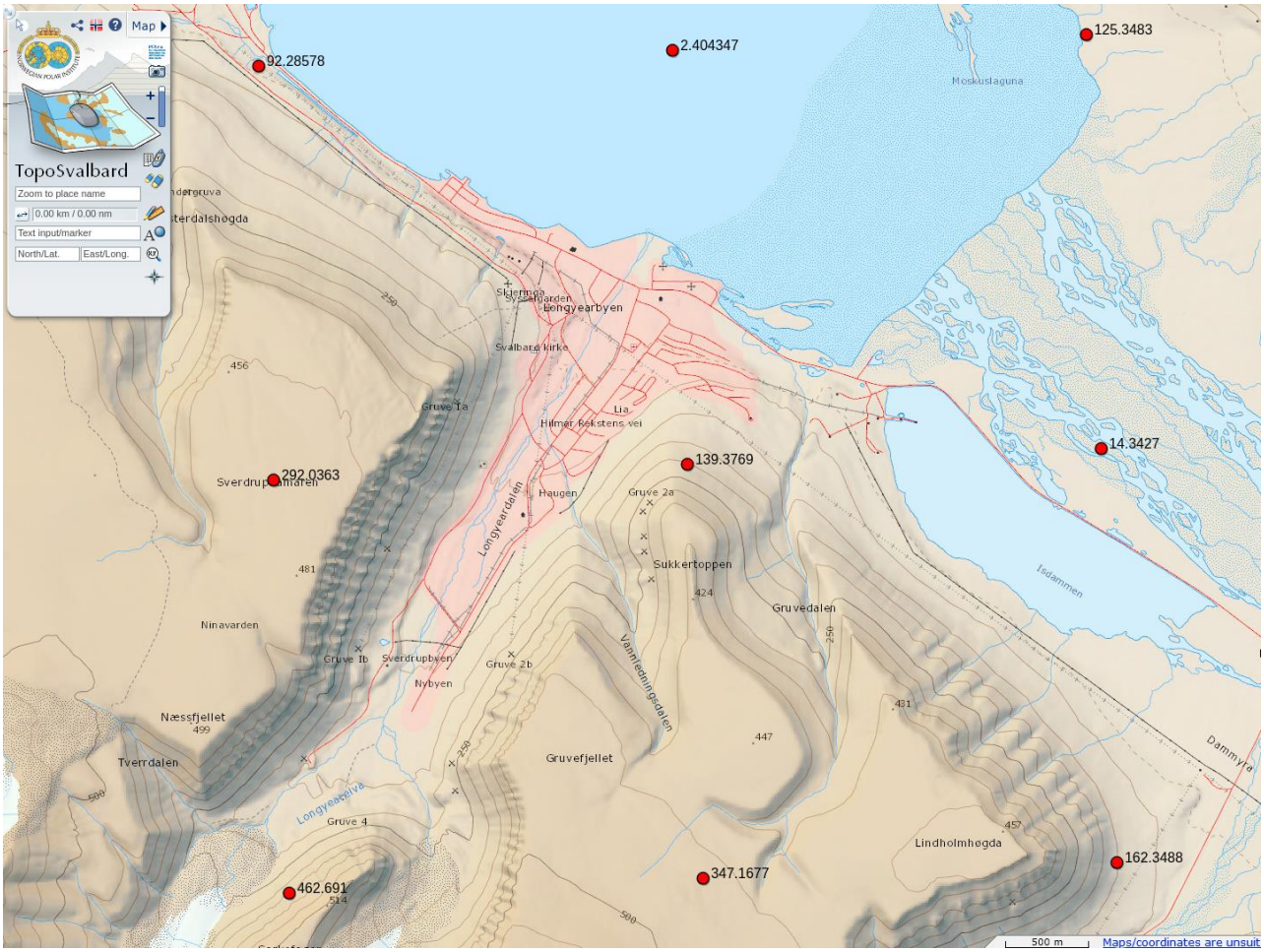

Figure 1: Geographical location of the climate data projection area overlaid on the map of Longyearbyen. The red dots show the center point of each grid in the 3x4 grid mesh. Map: © TopoSvalbard/Norwegian Polar Institute.

2.2 Near-Surface Air Temperature

The dataset provides insights into the near-surface air temperatures for the SVALBARD25 domain (Landgren et al., 2025). The dataset offers a comprehensive view of the annual mean air temperature, historical and projected, 2 meters above the ground from 1991 to 2070. The data was collected with a temporal frequency of every 3 hours, ensuring a detailed representation of temperature changes throughout each day. The data are for Longyearbyen area.

Upon examining the original dataset, several statistical observations were made. The mean temperature of the data was approximately -3.1 °C. The recorded temperatures varied, with the lowest reaching −45.2 °C and the highest peaking at 19.5 °C. This range of temperatures showcases the vast climatic variations in the region. Furthermore, the standard deviation, a measure of temperature variability, was found to be 9.1 °C.

In addition to the above observations, the mean annual temperatures were calculated by averaging the temperatures for each year across all coordinates (latitude and longitude). The average of these annual mean temperatures was −3.0 °C. Throughout the years, the annual temperatures fluctuated between −8.1 °C and 3.1 °C. The standard deviation for these annual mean temperatures was 1.9 °C, which provides insight into the variability of annual temperatures over the years.

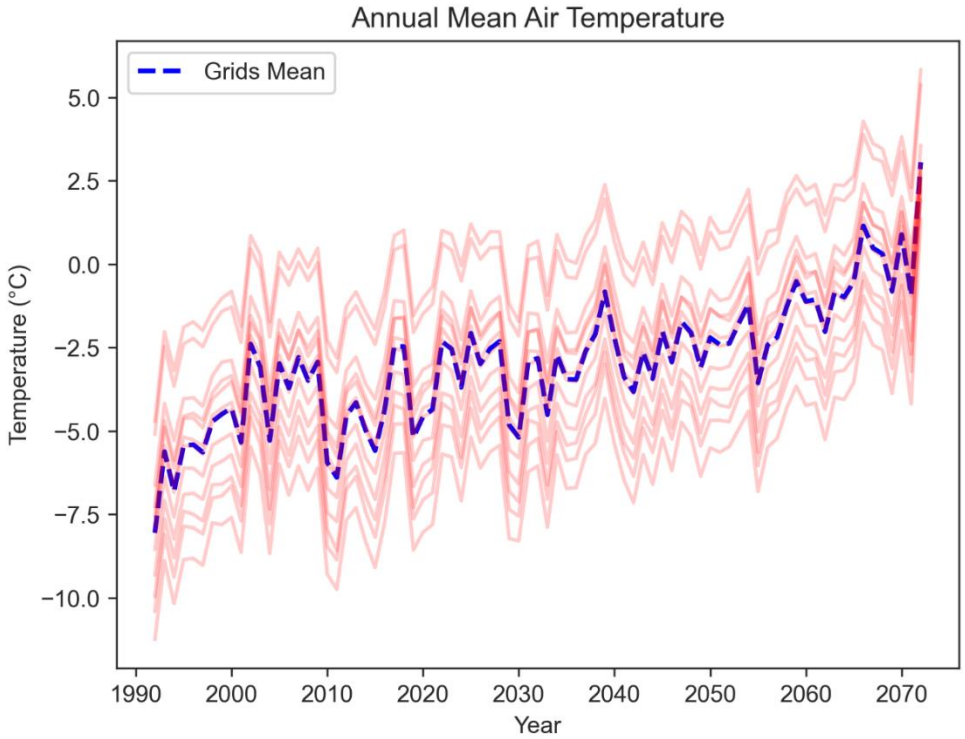

Figure 2: Annual mean air temperature versus year from Longyearbyen for the 12 grid points in Figure 1 for the climate data with the mean of all grids shown in a dashed line.

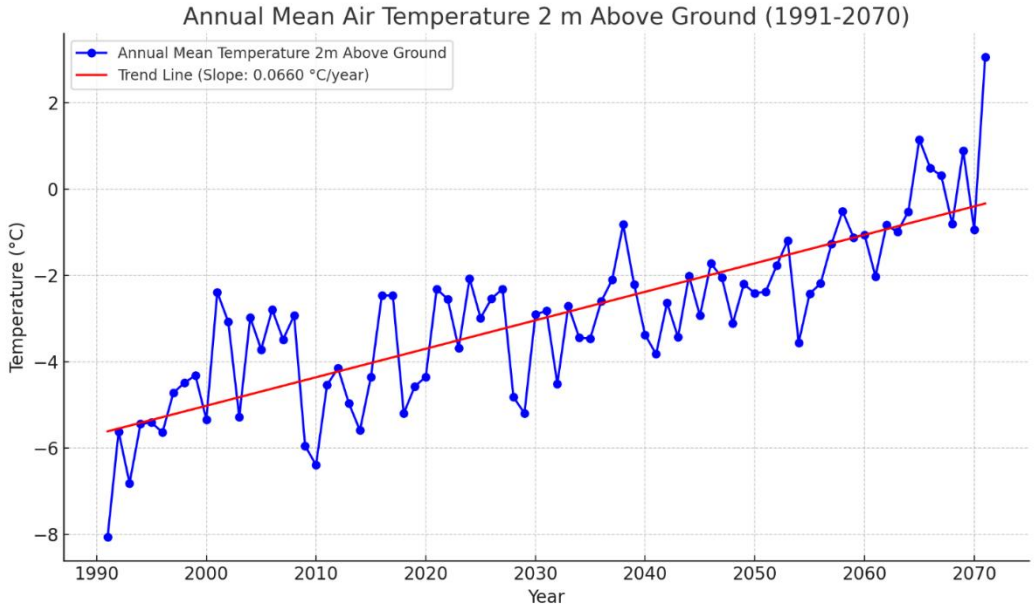

Figure 3: Trend analysis of the annual mean air temperature indicating a warming trend in Longyearbyen.

A linear regression analysis performed on this data shows cases of a pronounced warming trend, with the temperature rising at an average rate of approximately 0.07 °C per year. The positive slope of the regression line emphasizes this consistent increase over the eight-decade period. Moreover, the coefficient of determination, R^2, is estimated at 0.65. This signifies that the linear model accounts for about 65% of the variability in the annual mean temperature, providing a good fit to the data.

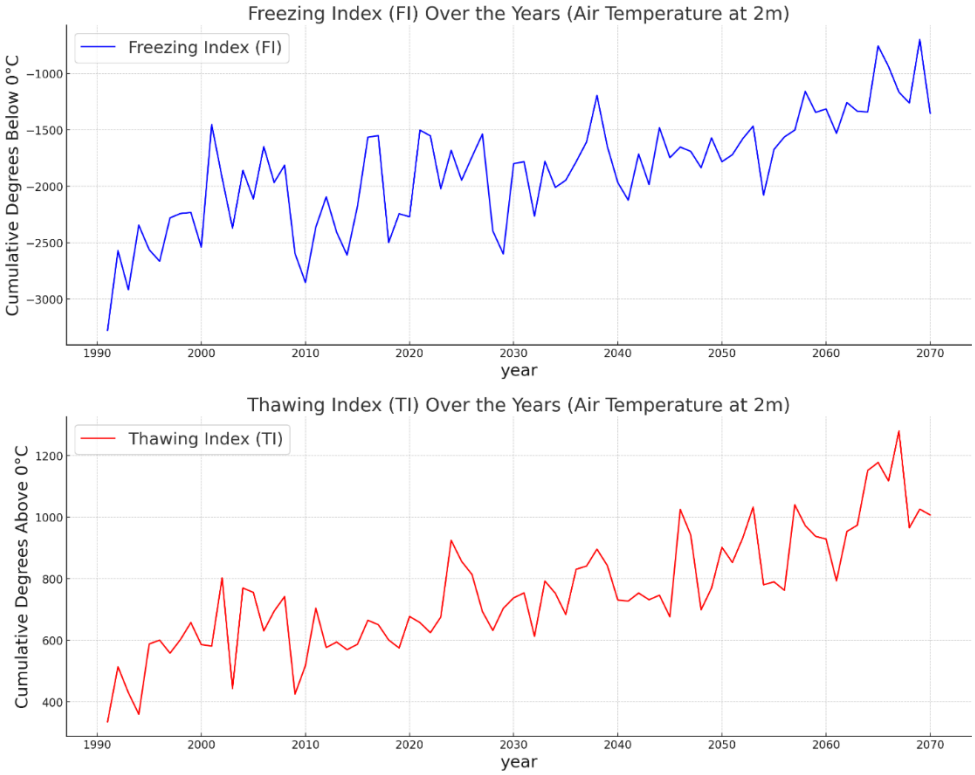

Figure 4: Freezing and thawing indices calculated based on the mean annual air temperature.

The provided plots depict the temporal evolution of the Freezing and Thawing Indices over an extensive period spanning from 1991 to 2070. These indices are crucial indicators in cold region studies as they offer insights into climatic patterns and potential impacts on the environment and infrastructure.

The **Freezing Index (FI)**, represented in blue on the top plot, quantifies the cumulative degree days below 0 °C each year. A higher Freezing Index implies a colder winter, which can lead to deeper ground freezing and more stable permafrost that potentially contributes to stability of historical infrastructure.

The **Thawing Index (TI)**, illustrated in red on the bottom plot, measures the cumulative degree days above 0 °C annually. A more substantial Thawing Index suggests a warmer summer. Warmer summers can lead to more extended thawing periods, impacting permafrost regions, leading to ground instability, which may potentially contribute to decreased stability of historical infrastructure.

A notable observation from the graphs is a potential trend suggesting decreasing freezing indices and increasing thawing indices over the decades. This could be indicative of a warming trend, aligning with global concerns regarding climate change. Such patterns necessitate proactive monitoring and adaptive strategies to address potential impacts on the environment, infrastructure, and communities in cold regions.

2.3 Surface Temperature

The dataset at hand offers a comprehensive look into the surface temperatures for the SVALBARD25 domain (Landgren et al., 2025). The dataset provides a detailed account of the surface temperature in Longyearbyen from 1991 to 2070. Recorded every 3 hours, the dataset captures the detailed fluctuations in temperature throughout each day.

Upon a close analysis of the dataset, several noteworthy statistics were observed. The average surface temperature was approximately −2.0 °C for the period. The temperature measurements exhibited significant variability, as evidenced by a notable standard deviation in the surface temperatures.

Further, the mean annual surface temperatures were determined by averaging temperatures for each year over all spatial coordinates. The resultant annual average was approximately −2.0 °C. These annual temperatures varied between −11.8 °C and 4.6 °C. Their standard deviation was 2.9 °C, highlighting the annual variability.

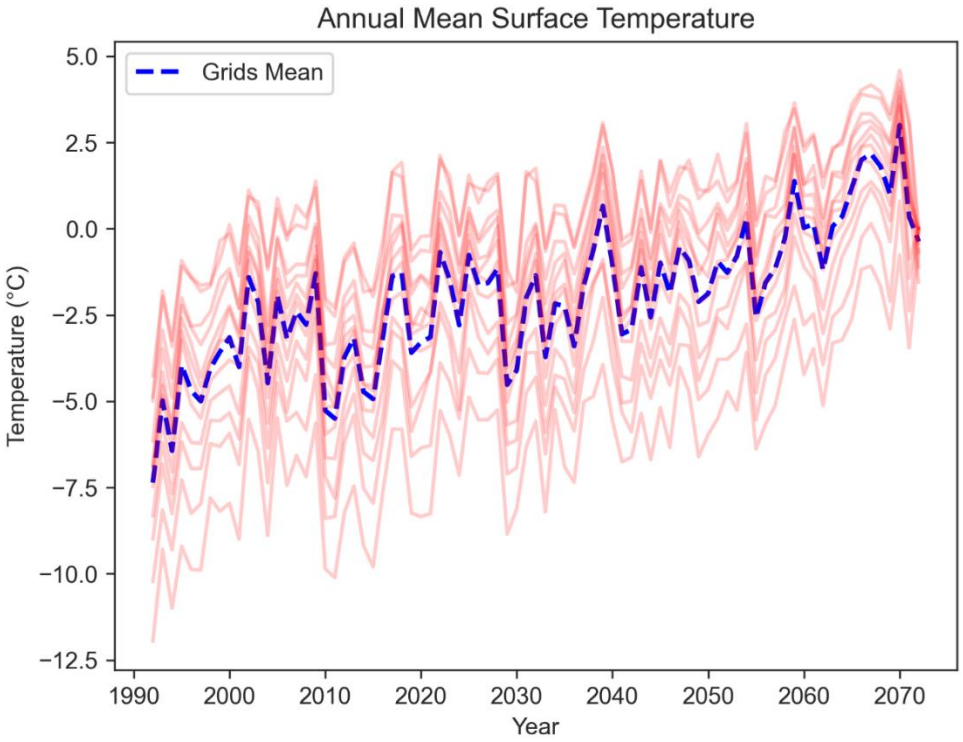

Figure 5: Annual mean surface temperature versus year for the 12 grid points in the climate data with the mean of all grids shown in a dashed line.

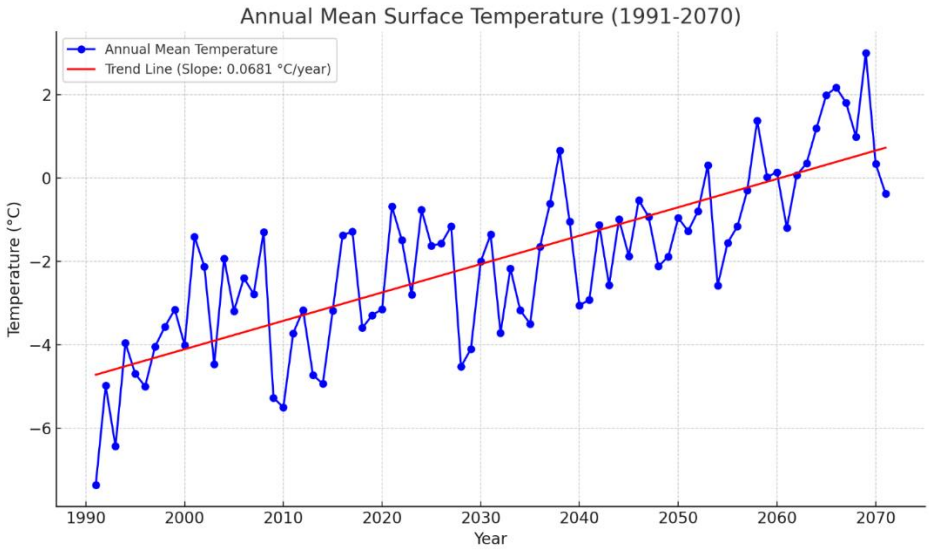

Figure 6: Trend analysis of the annual mean surface temperature indicating a warming trend, in Longyearbyen from 1990 to 2070.

A linear regression analysis of this data indicates a clear warming trend, with the temperature increasing at an average rate of approximately 0.07 °C per year. The positive slope of the trend line evidences this continuous rise over the studied period. The coefficient of determination, R^2, is approximately 0.62, suggesting that the linear model explains about 62% of the variability in the annual mean temperature. This value highlights the moderate fit of the linear trend to the observed data.

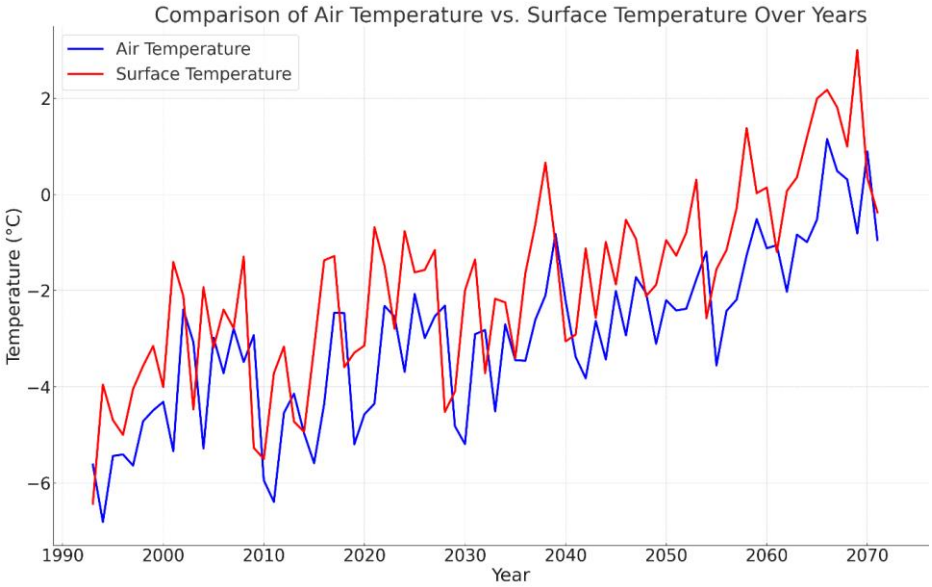

Figure 7: Comparison between air and surface temperature in Longyearbyen from 1990 to 2070.

From 1991 onwards, a comparison between air and surface temperatures presents notable patterns; Figure 7. Both temperature profiles display periodic fluctuations, presumably due to seasonal changes. However, a consistent trend emerges: the air temperature is predominantly lower than the surface temperature across the observed period. This suggests that the Earth's surface, possibly influenced by direct solar radiation, tends to be warmer than the immediate atmosphere above. The occasional overlaps and intersections in the temperature curves highlight the complex interplay of environmental factors. Observing such trends emphasizes the significance of understanding the disparities between atmospheric and ground-level thermal conditions.

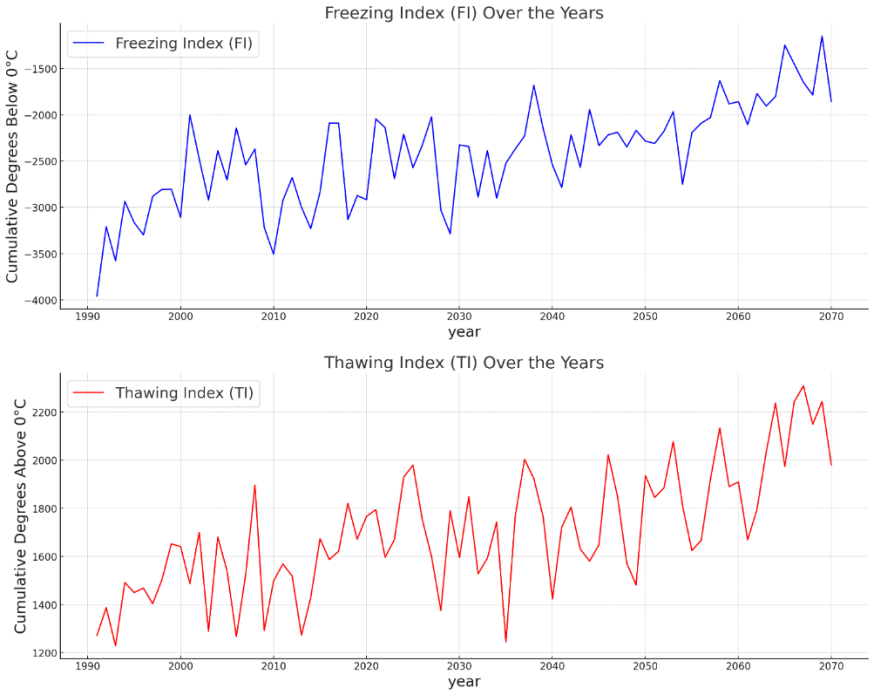

Figure 8: Freezing and thawing indices calculated based on the mean annual surface temperature.

Similar plots of FI and TI are generated for the surface temperature. Upon observation, both indices exhibit significant variability over the years. Notably, there seems to be a gradual decrease in the Freezing Index

and a corresponding increase in the Thawing Index over the years, indicating a potential warming trend. This pattern underscores the importance of ongoing monitoring and adaptive strategies to mitigate the potential impacts of climate change in cold regions.

2.4 Ground Temperature

The dataset provides ground temperature data from 1991 to 2070 across 14 distinct soil depth intervals: 0-1 cm, 1-4 cm, 4-10 cm, 10-20 cm, 20-40 cm, 40-60 cm, 60-80 cm, 80-100 cm, 1-1.5 m, 1.5-2 m, 2-3 m, 3-5 m, 5-8 m, and 8-12 m. Each layer's temperature data is furnished with a temporal resolution of three hours and is spatially distributed across a grid of varying longitude and latitude points.

To gain insights into the temporal dynamics of ground temperature, we computed the annual mean temperature for each depth layer throughout the entire time span. This approach facilitated a clearer understanding of temperature trends over the years for each specific depth layer.

This time series plot elucidates the evolution of ground temperature for each depth layer from 1991 to 2070. For each layer, a distinct trend line is presented, showcasing the annual mean temperatures. To provide a clearer understanding of the general trajectory, linear regression trend lines were overlaid on each time series.

The plot reveals a discernible warming trend across all layers over the analysed years. While all layers exhibit an increase in temperature, the rate of this increase is not uniform. Some layers present a more pronounced warming trend than others, suggesting that certain depths may be more susceptible to external temperature variations or other environmental factors.

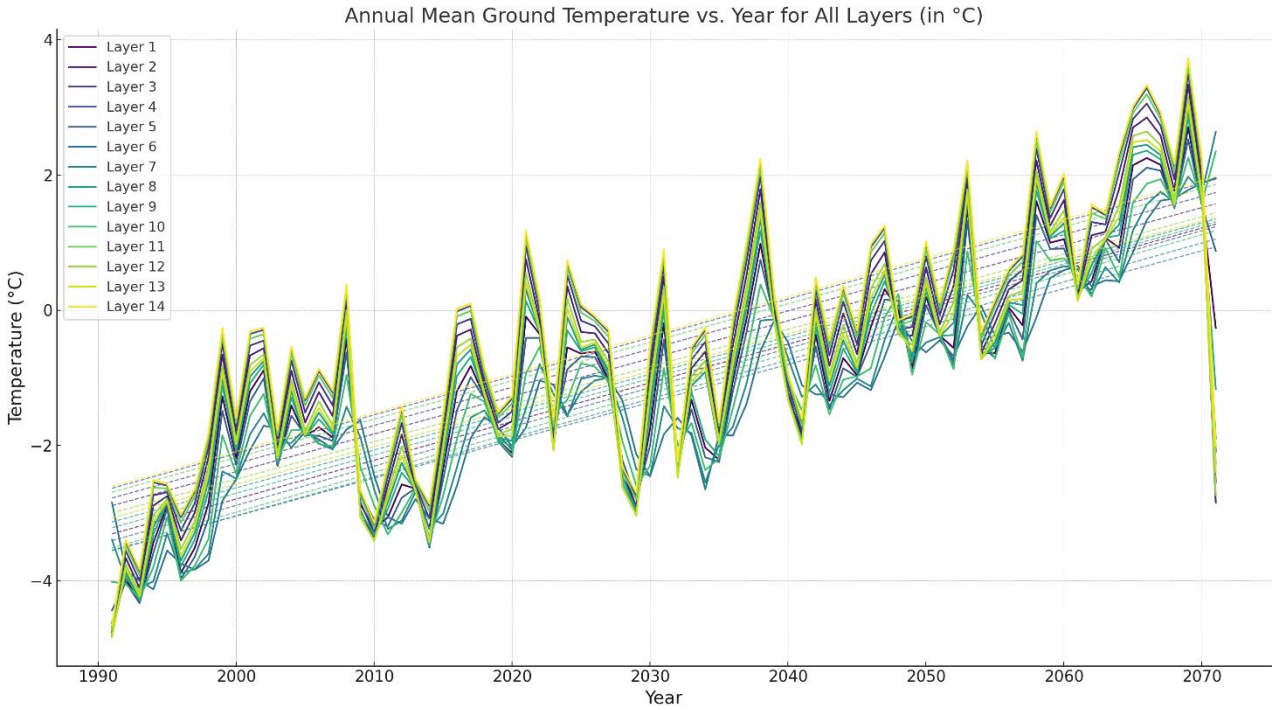

Figure 9: Ground temperature projections included in the climate data (Longyearbyen). Note that these ground temperature forecasts are included as a reference only to indicate the projected warming trend. Detailed forecasting of the ground temperature based on engineering numerical simulations is presented in the next chapter.

3 Ground Thermal Regime

3.1 Introduction

As the global climate undergoes transformative changes, one of the most pronounced and concerning effects is the degradation and warming of permafrost in cold regions. These changes not only threaten the structural integrity of infrastructure built upon them but also have profound implications for global carbon cycles, as previously trapped methane and carbon dioxide are released. Concurrently, there's a significant increase in active layer thicknesses, further intensifying the urgency to understand and predict these alterations. In this context, ground thermal simulations become indispensable. Temp/W, a leading tool in this domain, is used to provide predictions and insights into these phenomena. Simulations have been performed with Temp/W to investigate the thermal processes in the ground and their consequences on permafrost degradation and the associated increase in active layer thicknesses. In the following sections, the modeling assumptions, methodologies, and key findings are presented.

3.2 Theoretical Background of Temp/W

Temp/W operates on the foundation of the principles of heat transfer within porous media. At its core, the software utilizes the governing differential equations for heat conduction and advection in soils and rocks, offering both steady-state and transient solutions.

Heat Conduction: It is the process by which heat is transferred within a body due to a temperature gradient. The equation governing this is derived from Fourier's Law of Heat Conduction:

$$q = -k\nabla T$$

where q is the heat flux vector, k is the thermal conductivity, and ∇T represents the temperature gradient.

Heat Advection: In porous media, the movement of fluid can carry heat from one place to another, a process known as advection. The advective heat transfer is represented by:

$$q_{adv} = \rho c v \Delta T$$

where ρ is the fluid density, c is the specific heat, v is the fluid velocity, and ΔT is the temperature difference.

Boundary Conditions: Temp/W allows the application of various boundary conditions, including prescribed temperatures, heat fluxes, and convective boundaries, which are essential for simulating real-world scenarios effectively.

Numerical Solution: Temp/W employs the finite element method (FEM) to discretize the governing equations and solve them numerically. This approach enables it to handle complex geometries and heterogeneous material properties seamlessly.

While the software masks much of the complex mathematical machinery behind a user-friendly interface, it's grounded in these fundamental heat transfer principles and numerical methods, ensuring accuracy and reliability in its simulations.

3.3 Model Setup

3.3.1 Model Geometry

For the purposes of our study, an idealized model geometry was employed to perform the analysis and focus on the underlying thermal evolution. The chosen geometry for the model is depicted in Figure 10. It consists of a two-dimensional rectangular domain, spanning a width of 10 m and a height of 20 m. To ensure computational efficiency and resolution in capturing thermal variations, the model has been spatially discretized using an element size of 0.5 m. Given the simplicity of the model's geometrical properties and the consistency of its initial and boundary conditions, a uniform mesh size was deemed sufficient for our simulation requirements.

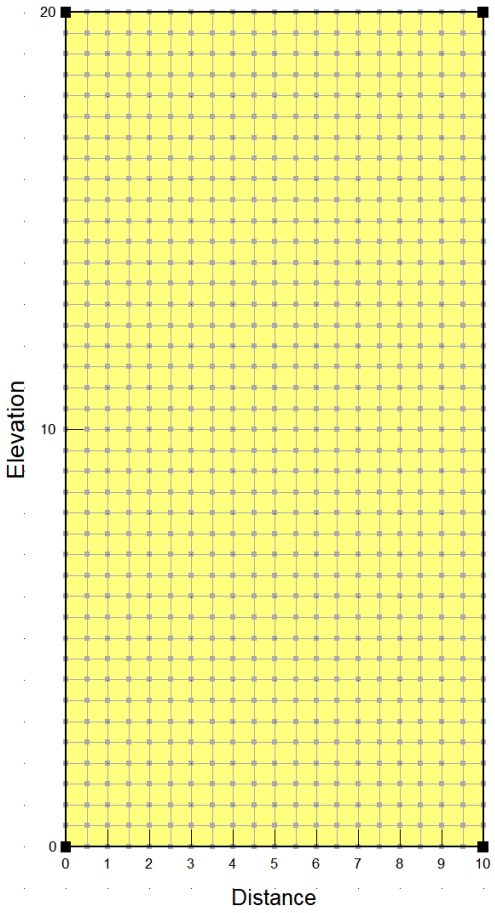

Figure 10: Model geometry used for thermal simulations in Temp/W.

3.3.2 Material Properties

A homogeneous material is assumed for the entire model geometry. The soil is assumed to be an ice-rich silt. The full thermal model from Temp/W is used to define the thermal properties of the soil. The material properties used from the simulations are presented in Table 1. The frozen thermal conductivity is slightly higher than the unfrozen thermal conductivity due to the higher thermal conductivity of ice compared to water (2.2 W/m/K versus 0.6 W/m/K). Conversely, the volumetric heat capacity of an unfrozen soil is higher than that of a frozen soil due to the higher volumetric heat capacity of water compared to ice.

Table 1: Material properties used for the thermal simulations in Temp/W.

Parameter	Value	Unit
Unfrozen thermal conductivity	1.60	W/m/K
Frozen thermal conductivity	1.76	W/m/K
Unfrozen volumetric heat capacity	3200	kJ/m^3/K
Frozen volumetric heat capacity	2400	kJ/m^3/K
In-situ volumetric water content	30	%

The unfrozen water content versus temperature curve for the soil is shown in Figure 11. The soil is assumed to contain some level of unfrozen water below the freezing temperature, gradually decreasing as the temperature decreases further.

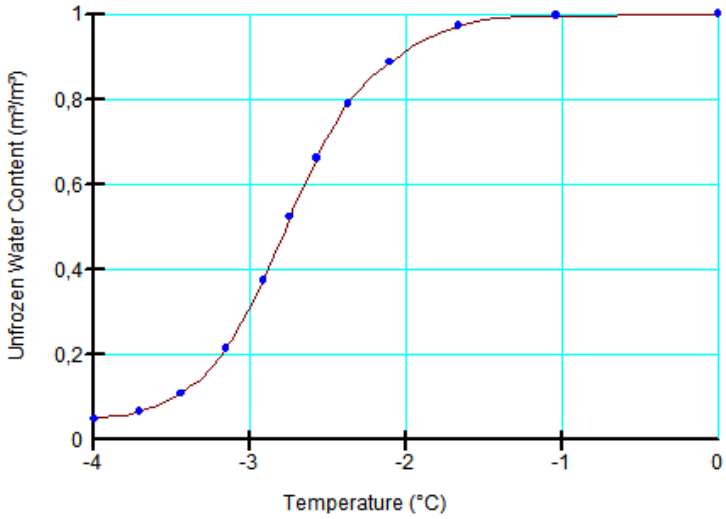

Figure 11: Unfrozen water content versus temperature used for the thermal simulations.

3.3.3 Initial Condition

In the absence of direct ground temperature measurements, establishing accurate initial conditions for thermal simulations presents a considerable challenge. To navigate this limitation, a method that leverages the temperature data from the period 1991-2000 has been employed as a basis for generating the initial state of the soil thermal profile. This decade serves as a representative baseline, reflecting the prevailing climatic conditions and setting the stage for the subsequent simulations spanning 2001-2070.

Given the lack of precise historical soil temperature records, the simulation starts with a pragmatic assumption: initializing the soil temperature profile with a uniform value of -5 °C. This value, though arbitrary, provides a reasonable starting point representing a typical permafrost condition. Using this as a foundation, the simulation integrates the surface boundary condition informed by the 1991-2000 temperature data. Over time, as the model iteratively processes the yearly temperature data, any potential inaccuracies stemming from this initial assumption are anticipated to diminish. The model's ability to adapt and evolve based on the input data ensures that the eventual thermal profile becomes a more accurate representation of the ground temperatures, even if the starting point is an estimation.

3.3.4 Boundary Conditions

In assessing long-term trends in active layer thicknesses and permafrost temperatures for regions like Svalbard, the selection of temperature boundary conditions is of utmost importance. Three distinct methodologies come to the fore: employing daily mean temperatures, adopting monthly mean temperatures, and utilizing seasonal mean temperatures.

Daily mean temperatures offer detailed day-to-day fluctuations, effectively capturing short-term weather anomalies such as high temperature days or unusually cold spells. While they do provide a granular view and can depict transient phenomena, they come with increased computational demands. Furthermore, there is a risk of overemphasizing short-lived events, which might obscure the larger picture when the emphasis is on long-term trends.

Monthly mean temperatures offer a moderate resolution, adept at capturing the transitions between months while still emphasizing overarching trends. When deployed using a step function, it delineates a stepwise representation of the year, thus encapsulating the nuanced climatic changes with reduced computational intensity. Monthly mean temperatures strike a harmonious balance between the granularity of daily data and the broader perspective of seasonal averages.

Conversely, seasonal mean temperatures take a more generalized approach by consolidating temperature data over extended periods, such as the polar day, polar night, and transitional seasons. Seasonal averages are effective in emphasizing broad climatic patterns and are useful when studying to long term effect of climate change on permafrost.

Given our focus on long-term shifts in active layer thicknesses and permafrost temperatures in Svalbard, the seasonal mean temperatures approach is identified as the most suitable. This method addresses the importance of recognizing enduring climatic patterns, making it a sensible choice. Taking into account our objectives and the goal of capturing significant climatic shifts impacting the region, the seasonal mean approach is elected as the most suitable and representative boundary condition for the simulation.

Figure 12 illustrates the step function of seasonal mean temperatures from 1991 to 2000. Each temperature value remains constant over its respective season, creating a "step" appearance. This approach helps in clearly discerning the temperature for each season, emphasizing the variations and patterns within the decade. This step function is used to generate an initial condition for the subsequent simulations.

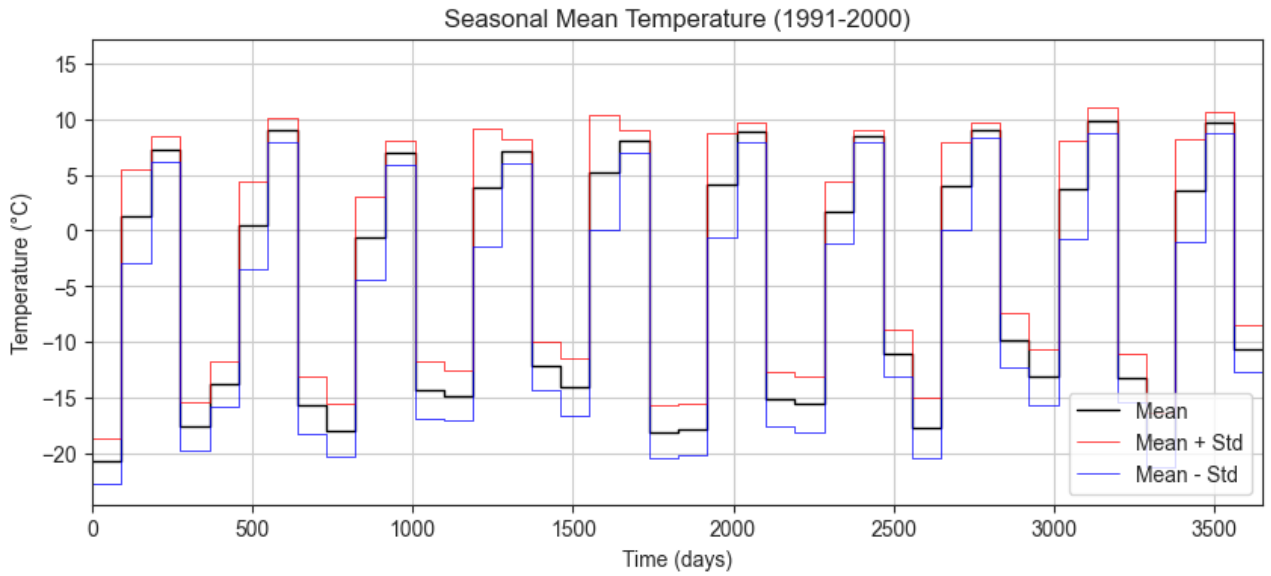

Figure 12: Monthly mean temperatures as a step function for the period from 1991 - 2000.

Figure 13 provides a close-up view of the seasonal mean temperatures for the years from 1991 and 1994, to provide a better illustration of the step function boundary conditions.

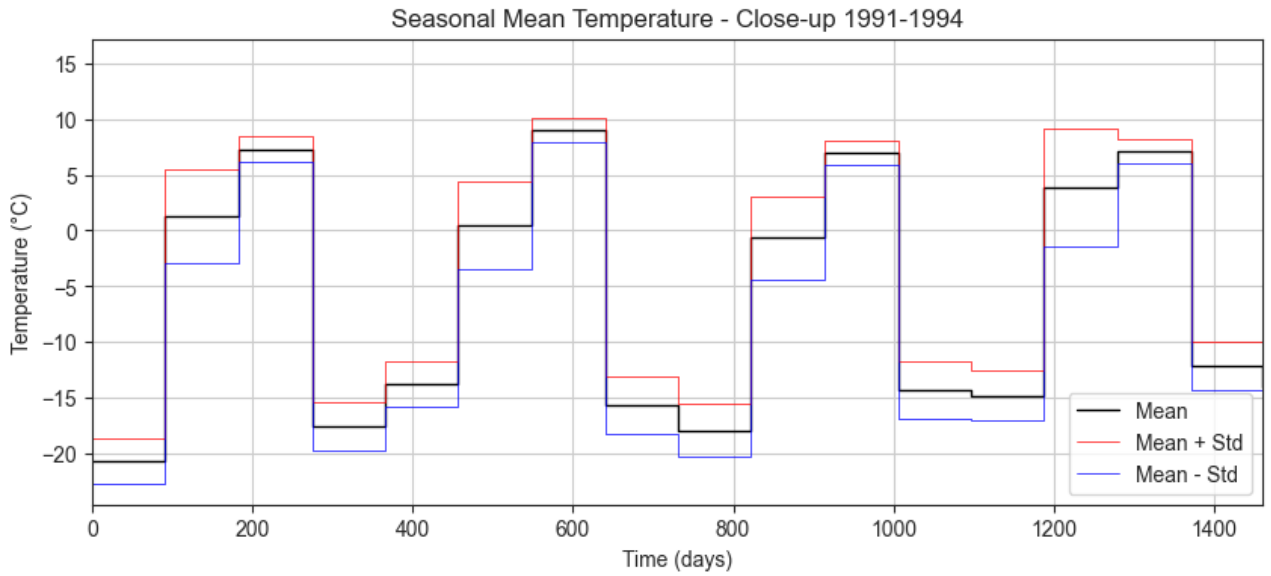

Figure 13: A close-up of the monthly mean temperatures as a step function for the years 1991 and 2001.

Figure 14 represents the step function of seasonal mean temperatures spanning from 2001 to 2070. This step function is used to drive the main ground temperature simulation and to forecast the evolution of active layer thicknesses and permafrost temperatures. It can be seen from the plot that the seasonal mean temperature increases steadily towards the year 2070.

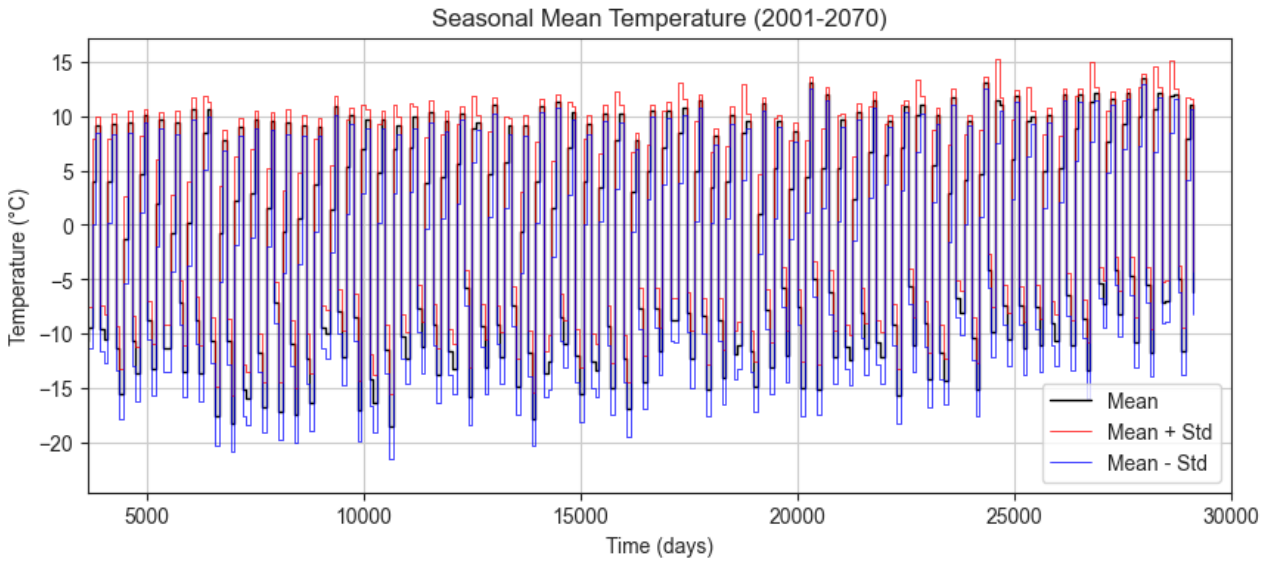

Figure 14: Monthly mean temperatures as a step function for the period from 2001 - 2070.

3.4 Results

3.4.1 Active Layer Thicknesses

For the simulations performed from 2001 to 2070, the active layer thicknesses are inferred from the warmest temperature profiles corresponding to each unique year. The collected results are plotted in terms of active layer thickness versus year plot shown in Figure 15. The overall trend is that active layer thicknesses increase from ca. 1.0 m in 2001 to more than 2.0 m during the year approaching 2070. The uncertainties in the projected active layer thicknesses are relatively high in the last decade considered (i.e. 2060 – 2070) due to the very high standard deviations observed in the projected temperature data. In the worst-case scenarios, active layer thicknesses up to or more than 3.0 m may be observed.

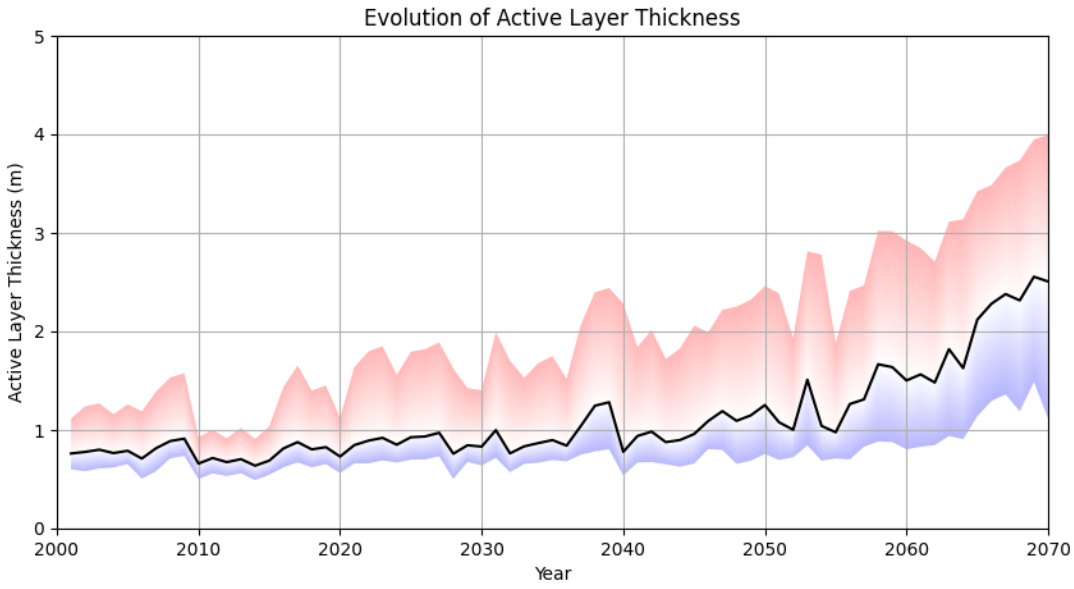

Figure 15: Evolution of active layer thickness for the period from 2001 to 2070. The solid black line represents the mean active layer thickness estimates, and the shaded regions represent the associated uncertainties.

3.4.2 Permafrost Temperatures

For the simulations from 2001 to 2070, the permafrost temperature evolutions are investigated by extracting the warmest and coldest temperature profiles for each unique year. The temperature profiles for the year 2023 are first extracted and the results are shown in Figure 16. This serves to control the reliability of the thermal simulation results. Literature data indicate that the permafrost temperature in lowland areas around and within Longyearbyen is around -4 °C to -5 °C while the active layer thickness is around 1.0 m, (Christiansen et al., 2019) and (Gilbert et al., 2019). The temperature profiles from the simulations for the year 2023 are close to these values, which building confidence in the reliability of the results and the simulation approach.

Future temperature profiles with depth are extracted for the years 2040, 2050, 2060 and 2070. The temperature profiles for the years 2040 and 2050 are shown in Figure 17 while those for 2060 and 2070 are shown in Figure 18. In line with the increasing active layer thicknesses, the permafrost temperature at 20 m depth shows a steady increase from around -4.3 °C in 2023 to ca. -3.2 °C by the end of 2070. The uncertainties in the projected permafrost temperatures are relatively smaller compared to the uncertainties in the active layer thicknesses.

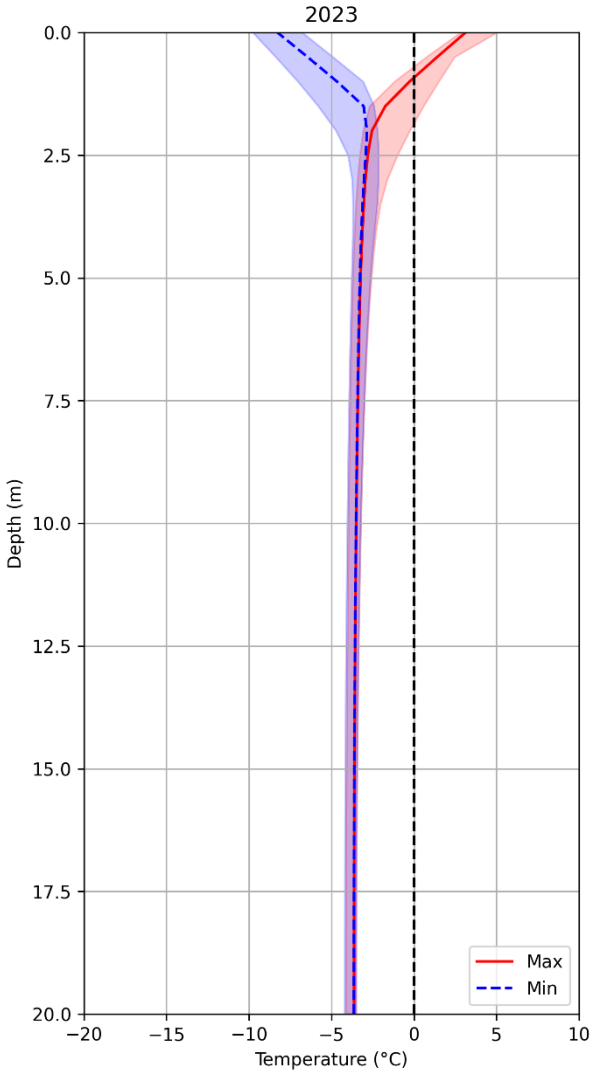

Figure 16: Warmest and coldest ground temperature profiles for the year 2023.

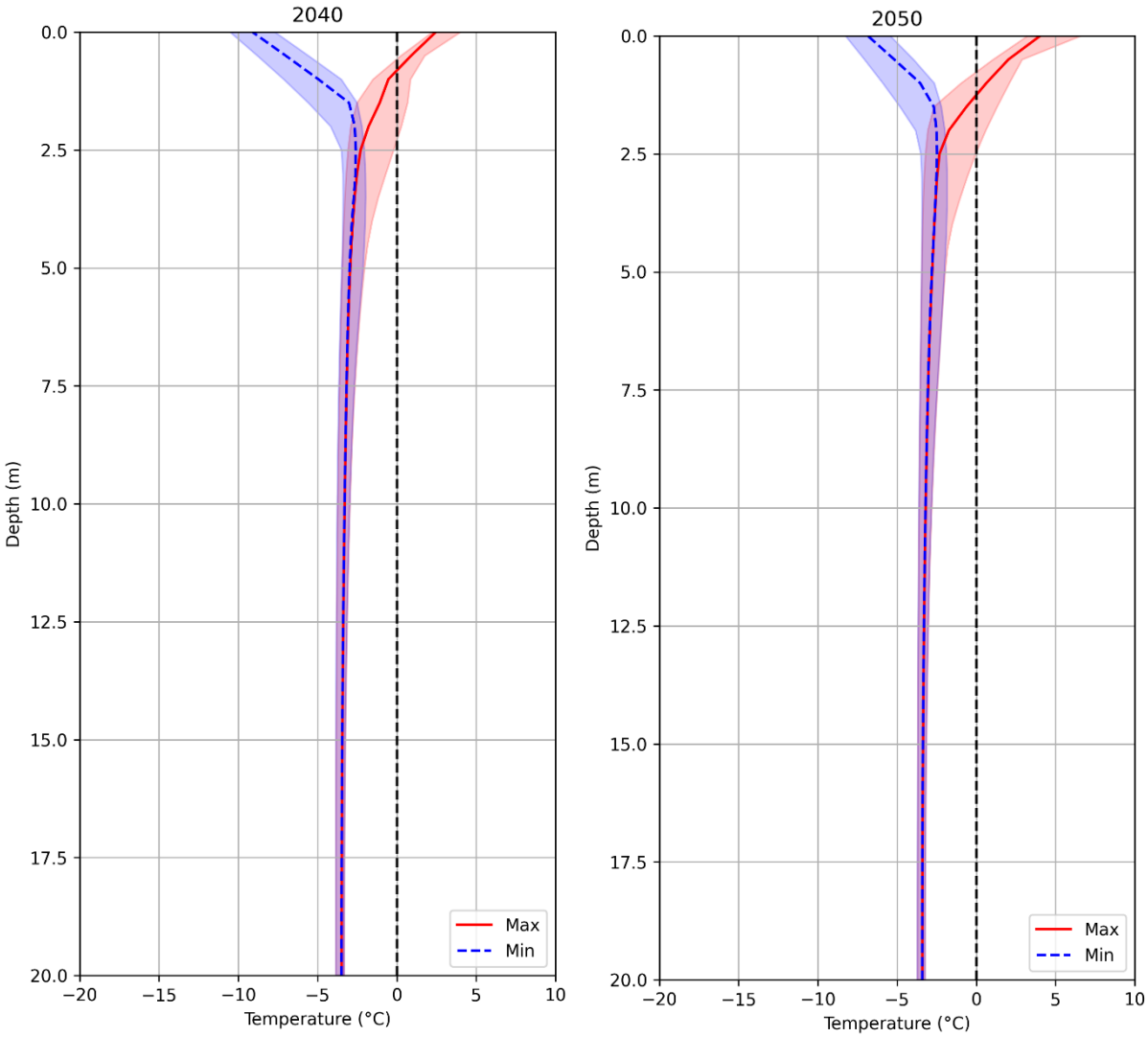

Figure 17: Warmest and coldest ground temperature profiles for the years 2040 and 2050.

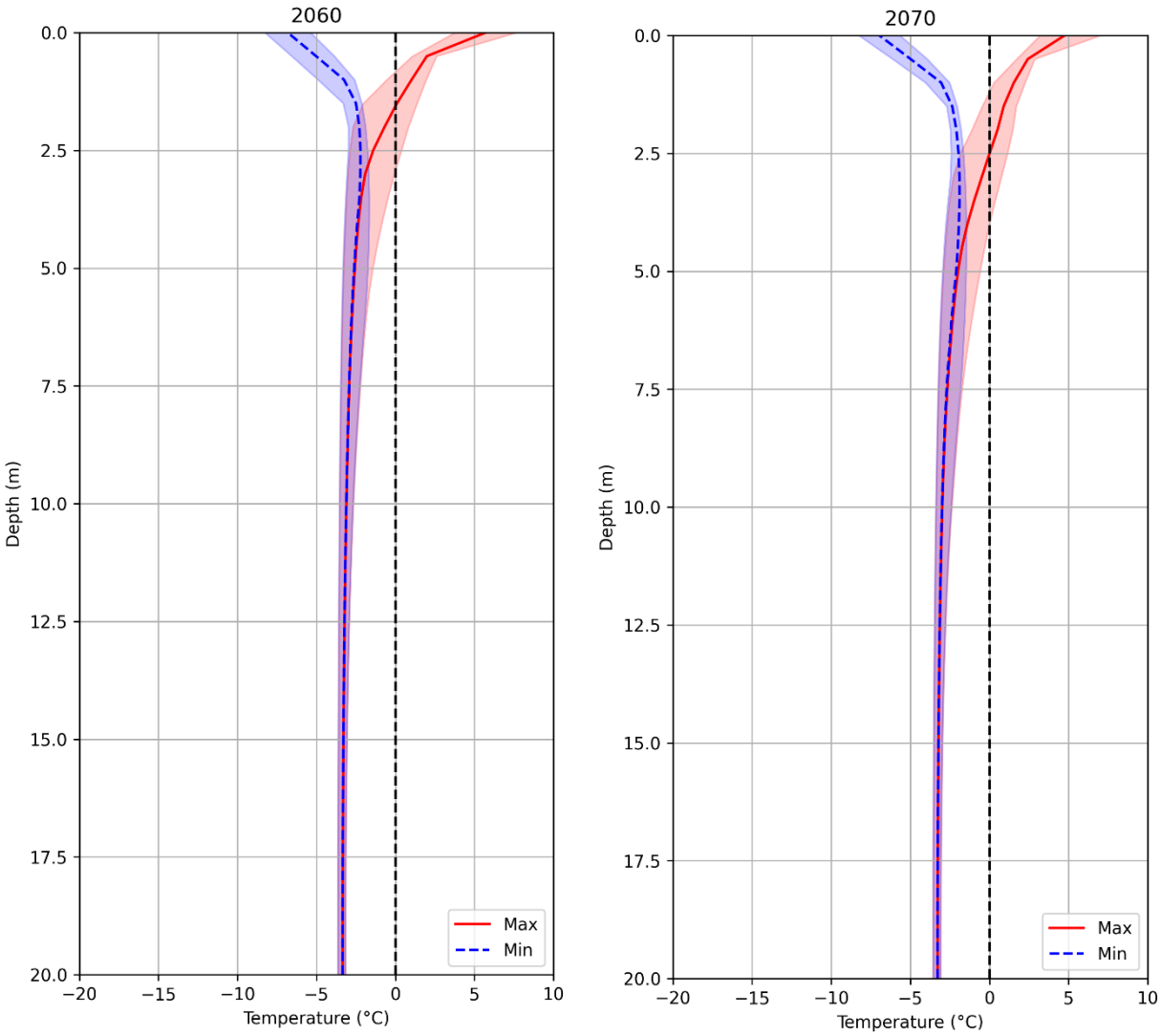

Figure 18: Warmest and coldest ground temperature profiles for the years 2060 and 2070.

4 Probabilistic Analysis of Pile Foundation Capacity

4.1 Design Approaches for Axially Loaded Piles

There are two alternative design approaches for axially loaded piles in permafrost: limiting shear stress and limiting settlement rate (Andersland and Ladanyi, 2003). The choice of approach depends on the specific site conditions and the desired level of safety and serviceability. The two approaches are:

1. **Limiting Shear Stress**: This approach is based on the assumption that excessive shear stress along the pile shaft can lead to significant settlement and damage to the pile. The acceptable shear stress is determined based on the site soil conditions and the desired safety factor. This approach is typically used when the pile is driven to a depth where the permafrost is relatively shallow and the pile is not subjected to large lateral loads. End bearing is considered in design only when the pile tip is driven to rock or dense sands or gravels. This is because the shear strength of permafrost is typically much lower than that of rock or dense sands or gravels.
2. **Limiting Settlement Rate**: This approach is based on the assumption that excessive settlement can lead to structural or functional problems with the supported structure. The acceptable settlement rate is determined based on the service life of the structure and the desired serviceability criteria.

The focus of this chapter is on the limiting shear stress approach to estimate the capacity of axially loaded piles.

4.2 Capacity of Axially Loaded Single Piles

4.2.1 Factors Affecting Pile Capacity

The ability of single piles embedded in permafrost to withstand static vertical loads is influenced by several key factors:

- **Permafrost temperature**: The temperature profile of the permafrost, particularly its warmest or average state, plays a crucial role in determining the pile's capacity. A warmer permafrost may experience reduced adfreeze strength and increased susceptibility to thawing, potentially leading to instability.
- **Adfreeze strength**: The bond strength between the pile and the frozen soil, known as adfreeze strength, is significantly affected by permafrost temperature. Sufficient adfreeze strength is essential for the pile to withstand loads without excessive movement.
- **Embedment length**: The length of the pile's embedment in the permafrost must be sufficient to carry the imposed loads and resist forces such as downdrag and frost heaving. Adequate embedment ensures the pile's stability and ability to handle the dynamic nature of permafrost environments.
- **Pile type and construction**: The type and size of the pile, along with the specific construction procedures employed, significantly impact its performance. Factors like pile geometry, material properties, and driving methods influence the pile's ability to integrate with the permafrost and withstand stress.
- **Freeze-back**: Ensuring complete freeze-back of the permafrost before applying loads is essential. A fully frozen permafrost provides a stable and predictable foundation for the pile, ensuring its long-term integrity and reliability.

4.2.2 Adfreeze Strength

Adfreeze strength is the bond strength developed between the surface of a pile and the surrounding frozen soil. It is a key factor in determining the capacity of axially loaded piles in permafrost.

The capacity of a single pile resulting from adfreeze strength is given by

$$Q_a = A_s \cdot \tau_a$$

where τ_a is the adfreeze strength and A_s is the surface area of the pile in contact with frozen soil.

The adfreeze strength of frozen soils is related to the long-term shear strength τ_{lt} i.e.

$$\tau_a = m \cdot \tau_{lt}$$

where m is a factor accounting for pile roughness (depending on material type) and surficial characteristics. The values of this factor for different pile materials, proposed by (Weaver and Morgenstern, 1981), is presented in Table 2.

Table 2: Value of factor m for different pile materials, after (Weaver and Morgenstern, 1981).

Pile type	Factor m
Steel	0.6
Concrete	0.6
Timber (uncreosoted)	0.7
Corrugated steel pipe	1.0

The long-term shear strength of frozen soil involves frictional and cohesive components according to the Mohr-Coulomb criterion and can be expressed as

$$\tau_{lt} = c_{lt} + \sigma \cdot \tan \phi_{lt}$$

where c_{lt} represents the long-term cohesion, σ the normal stress on the shear plane and ϕ_{lt} the friction angle. Since the normal stress on the shear plane is usually small compared to the long-term cohesion, it is usually neglected. This reduces the above equation to

$$\tau_{lt} = c_{lt}$$

Thus, the adfreeze strength can be expressed as

$$\tau_a = m \cdot c_{lt}$$

This implies that the long-term cohesion is the most important parameter in defining the axial capacity for a pile in permafrost. Based on data from different tests and locations, (Weaver and Morgenstern, 1981) have summarized the likely long-term cohesion values for different types of soil. These values are shown in the plot in Figure 19.

A model for the long-term cohesion is presented by (Tsegaye, A.B., Guegan, E. Nordal, S., 2015). We present a modified version of the model here and express the long-term cohesion as

$$c_{lt} = c_t + \frac{\rho_w L_f}{T_f} \cdot \beta \cdot \langle T_f - T \rangle^{1-\alpha}$$

where c_t is the thawed cohesion, ρ_w is the density of water, L_f is the latent heat of fusion, T_f is the freezing temperature, T is the temperature of the permafrost and α and β are model parameters. Note that $\langle \cdot \rangle$ represent the Macaulay brackets where

$$\langle T_f - T \rangle = \begin{cases} 0, & T_f < T \\ T_f - T, & T_f \geq T \end{cases}$$

In other words, the long-term cohesion reduces to the thawed cohesion for temperatures above the freezing temperature. The model parameters α and β help to account for properties such as porosity and water content, which have an impact on the cohesive strength of a soil. Thes parameters may be estimated based on the expected long-term cohesions presented in Figure 19.

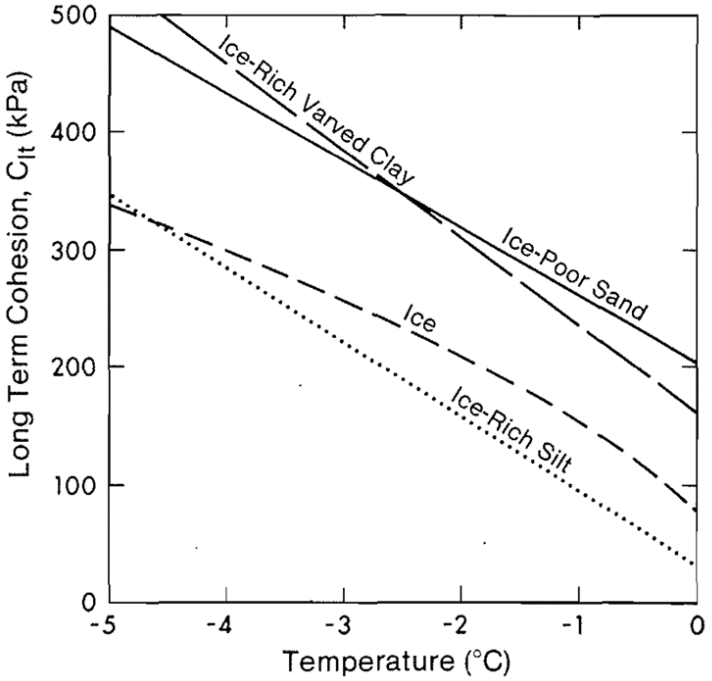

Figure 19: Long-term cohesion of frozen soil for different soil types, after (Weaver and Morgenstern, 1981).

4.2.3 Ultimate Pile Capacity

When the contribution from end bearing is neglected, the ultimate pile capacity for a single axially loaded pile will be equal to the capacity resulting from adfreeze strength i.e.

$$Q_u \approx Q_a = A_s \cdot m \cdot c_{lt}$$

The surface of the pile in contact with the frozen soil is

$$A_s = s \cdot L_{eff}$$

where s is the circumference of the pile and L_{eff} is the effective pile embedment length which is defined as the length of pile embedded in soil which is continuously below -1 °C. The effective embedment length can be expressed as

$$L_{eff} = L_g - \mu \cdot L_a$$

where L_g is the length of the pile below ground level, L_a is the active layer thickness and μ is a parameter that is introduced to find the point at which the permafrost temperature equals -1 °C below the active layer thickness. Combining the equations above gives

$$Q_u = s \cdot \left(L_g - \mu \cdot L_a\right) \cdot m \cdot c_{lt}$$

Using the model for long-term cohesion in the equation above results in

$$Q_u = s \cdot \left(L_g - \mu \cdot L_a\right) \cdot m \cdot \left[c_t + \frac{\rho_w L_f}{T_f} \cdot \beta \cdot \langle T_f - T \rangle^{1-\alpha}\right]$$

4.3 Probabilistic Pile Capacity Analysis

4.3.1 Probabilistic Parameters

The ultimate pile capacity equation for axially loaded single pile presented in the previous section involves several parameters for the soil and pile. In the context of performing probabilistic analysis for pile capacities, it is first important which parameters can be considered deterministic and which probabilistic. It can easily be concluded that most of the uncertainty in estimating the ultimate pile capacity stems from the values of the active layer thickness and the permafrost temperature. These parameters can thus be considered to be probabilistic.

Table 3: Deterministic and probabilistic parameters in the ultimate pile capacity model.

Parameter	Uncertainty Type	
	Deterministic	Probabilistic
Pile circumference, s	x	
Length of pile below ground, L_g	x	
Model parameter, μ	x	
Active layer thickness, L_a		x
Roughness coefficient, m	x	
Thawed cohesion, c_t	x	
Density of water, ρ_w	x	
Latent heat of fusion, L_f	x	
Freezing Temperature, T_f	x	
Model parameter, β	x	
Soil temperature, T		x
Model parameter, α	x	

The probabilistic parameters can then be presented in terms of a certain probabilistic distribution, usually the normal distribution, to perform probabilistic pile capacity analysis.

4.3.2 Probabilistic Analysis

The Monte Carlo method is an essential computational technique that utilizes repeated random sampling to approximate numerical solutions, particularly valuable in scenarios with significant uncertainties. This method is effectively employed in various engineering applications. Here we apply it for the probabilistic analysis of ultimate pile capacity. The key steps involved in applying the Monte Carlo method for ultimate axial pile capacity are:

- ***Definition of probabilistic parameters***: The first step involves identifying parameters that have inherent uncertainty. In the context of ultimate pile capacity, these parameters are the active layer thickness and the permafrost temperature. Each of these parameters is characterized by a probability distribution, typically a normal distribution.

- ***Simulation setup***: A computational model is developed incorporating both deterministic parameters (such as pile circumference, length of pile below ground, etc.) and the identified probabilistic parameters. This model calculates the ultimate pile capacity for given sets of parameter values.
- ***Random sampling process***: For each probabilistic parameter, a series of random values are generated based on the specified probability distribution. This is achieved using random number generators tailored to the distribution characteristics.
- ***Execution of simulations***: The model is run multiple times, each iteration utilizing a unique set of randomly sampled values for the probabilistic parameters. This step is central to the Monte Carlo method, enabling the exploration of the model's behaviour under varied conditions.
- ***Result analysis***: Upon conducting a substantial number of simulations, the outcomes are analyzed to derive the distribution of the ultimate pile capacity. This analysis typically includes the calculation of statistical metrics such as mean, median, standard deviation, and the creation of visual representations like histograms or probability density functions to depict the distribution of outcomes.
- ***Interpretation for decision-making***: The final step involves interpreting the results for informed decision-making. The distribution and statistical analysis of the ultimate pile capacity offer insights into the range and likelihood of different outcomes, aiding in risk assessment and strategic planning.

In the context of assessing the structural integrity of piles under axial loads, determining the probability of failure is a crucial aspect of risk management. This probability can be quantified using the distribution of ultimate pile capacity derived from Monte Carlo simulations.

Calculation of allowable load: The initial step involves computing the allowable load on the pile, which is determined by dividing the specified axial load by the factor of safety (FS) i.e.

$$Allowable\ load = Q_{req} = \frac{Q_{axial}}{FS}$$

Probability of failure estimation: The probability of failure is the likelihood that the pile's ultimate capacity is less than or equal to the allowable load. This probability is calculated as the cumulative probability up to the allowable load within the ultimate pile capacity distribution. Mathematically, it involves the integration of the probability density function from the minimum potential capacity to the allowable load. Alternatively, in a discrete dataset derived from simulation runs, it can be calculated as:

$$P_F = \frac{Number\ of\ simulations\ where\ capacity \leq Allowable\ load}{Total\ number\ of\ simulations} \cdot 100$$

The obtained probability of failure is a crucial metric for risk assessment. It provides a quantitative measure of the likelihood that the pile may fail under the given loading conditions, taking into account the applied factor of safety. A higher probability of failure may necessitate further investigations to mitigate risks.

4.4 Results

4.4.1 Demonstration Problem

We demonstrate the probabilistic analysis methodology presented in the previous sections through a simple example. We consider a timber pile with a diameter of 20 cm and a total length of 10 m below ground level. Assuming the soil type at the site is an ice-rich silt with a thawed cohesion of 20 kPa, the model parameters for the long-term cohesion model are estimated from curve fitting as $\alpha = 0.0031$ and $\beta = 0.0418$. The curve fitting is shown in Figure 20. These and other required parameters are summarized in Table 4.

A normal distribution is assumed for the probabilistic parameters i.e. the active layer thickness and the permafrost temperature. Thus, they are defined their mean and standard deviation values. Their values, based on the thermal analysis in the previous chapter, are presented in

Table 5.

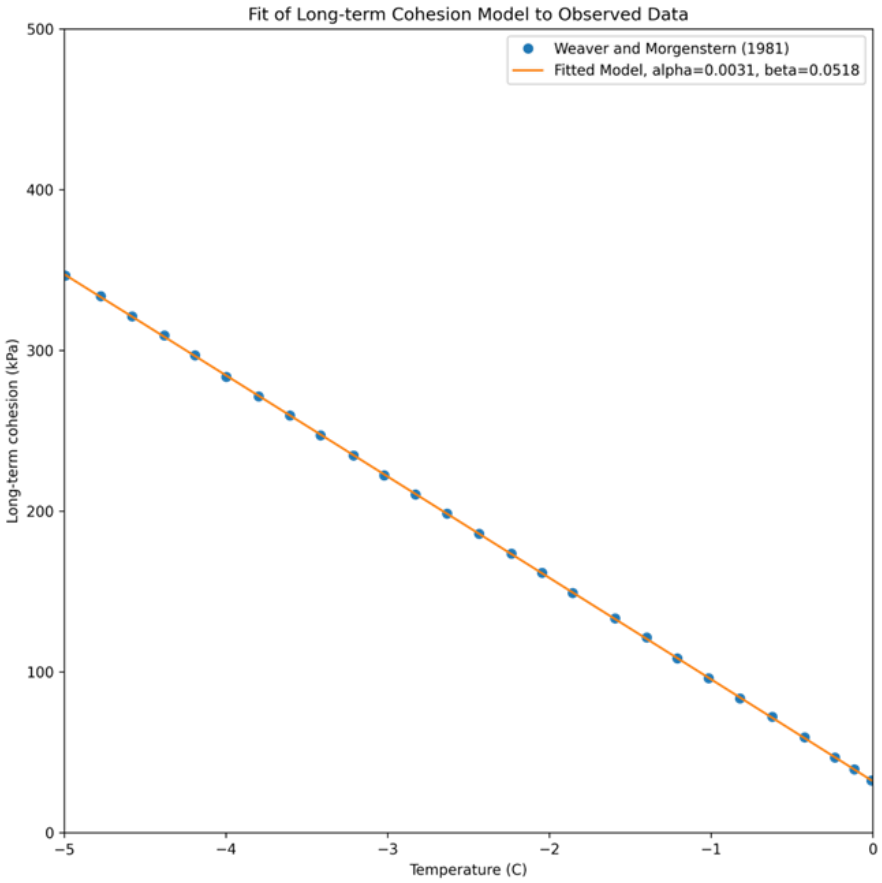

Figure 20: Curve fitting to obtain model parameters for the long-term cohesion of ice-rich silt.

Table 4: Values of deterministic parameters used for analysis.

Parameter	**Value**
Pile circumference, s	0.63 m
Length of pile below ground, L_g	10 m
Model parameter, μ	1.1
Roughness coefficient, m	0.7
Thawed cohesion, c_t	20 kPa
Density of water, ρ_w	1000 kg/m^3
Latent heat of fusion, L_f	334 kJ/kg
Freezing Temperature, T_f	273.15 K
Model parameter, β	0.0518
Model parameter, α	0.0031

Table 5: Values of probabilistic parameters used for analysis based on Figure 15.

Parameter	Mean Value	Standard Deviation
Active layer thickness, L_a	2.5 m	1.0 m
Permafrost temperature, T	-3.2 °C	1.2 °C

We assume that the axial load that needs to be supported by the pile is 250 kN with a safety factor of 2.0 i.e. failure is considered to occur if the estimated capacity of the pile is below 500 kN.

For the parameters considered above, Monte Carlo analysis with 10000 simulations results in the pile capacity distribution shown in Figure 21. For the required axial load to be carried, the axial capacity distribution implies a failure probability of 21.7%, which can be said to be significant.

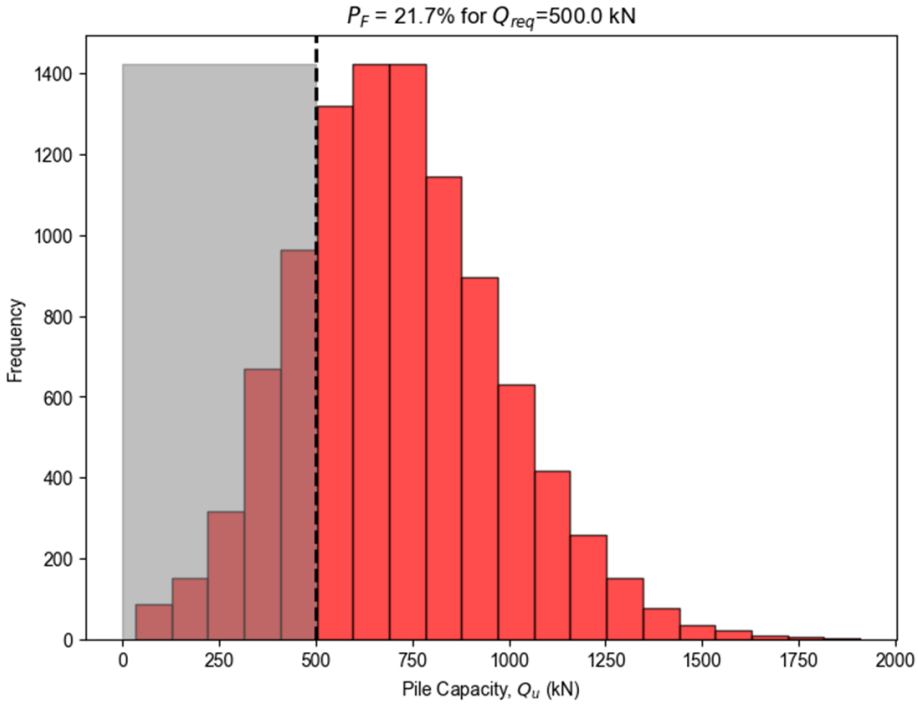

Figure 21: Probabilistic axial capacity distribution for active layer thickness $L_a = 2.5\ m \pm 1.0\ m$ and permafrost temperature $T = -3.2\ °C \pm 1.2\ °C$.

4.4.2 Sensitivity to Active Layer Thickness

To investigate the effect of the probabilistic parameters on the failure probability, sensitivity analysis is performed by varying the probability distributions of the parameters.

Sensitivity analysis is first performed with respect to the active layer thickness. We maintain a similar mean value 2.5 m (representing future climate scenarios) as in the previous section and consider four different standard deviations: 0.4 m, 0.8 m, 1.2 m and 1.6 m. The mean and standard deviation values for the permafrost temperature are kept the same as in the previous section i.e. as -3.2 °C and 1.2 °C, respectively.

The axial pile capacity distributions for the four different combinations of probabilistic parameters are shown in Figure 22. The two plots in the top row show the results for the active layer thickness $L_a = 2.5\ m \pm 0.4\ m$ and $L_a = 2.5\ m \pm 0.8\ m$ and those in the bottom row are for $L_a = 2.5\ m \pm 1.2\ m$ and $L_a = 2.5\ m \pm 1.6\ m$. We find that the failure probabilities are 6.5%, 7.9%, 9.2% and 12.2% (which are significantly high values in the context of reliability-based design) for the four different active layer thickness distributions, respectively with their standard deviations in increasing order. A higher active layer thickness, with other parameters remaining the same, increase the failure probability.

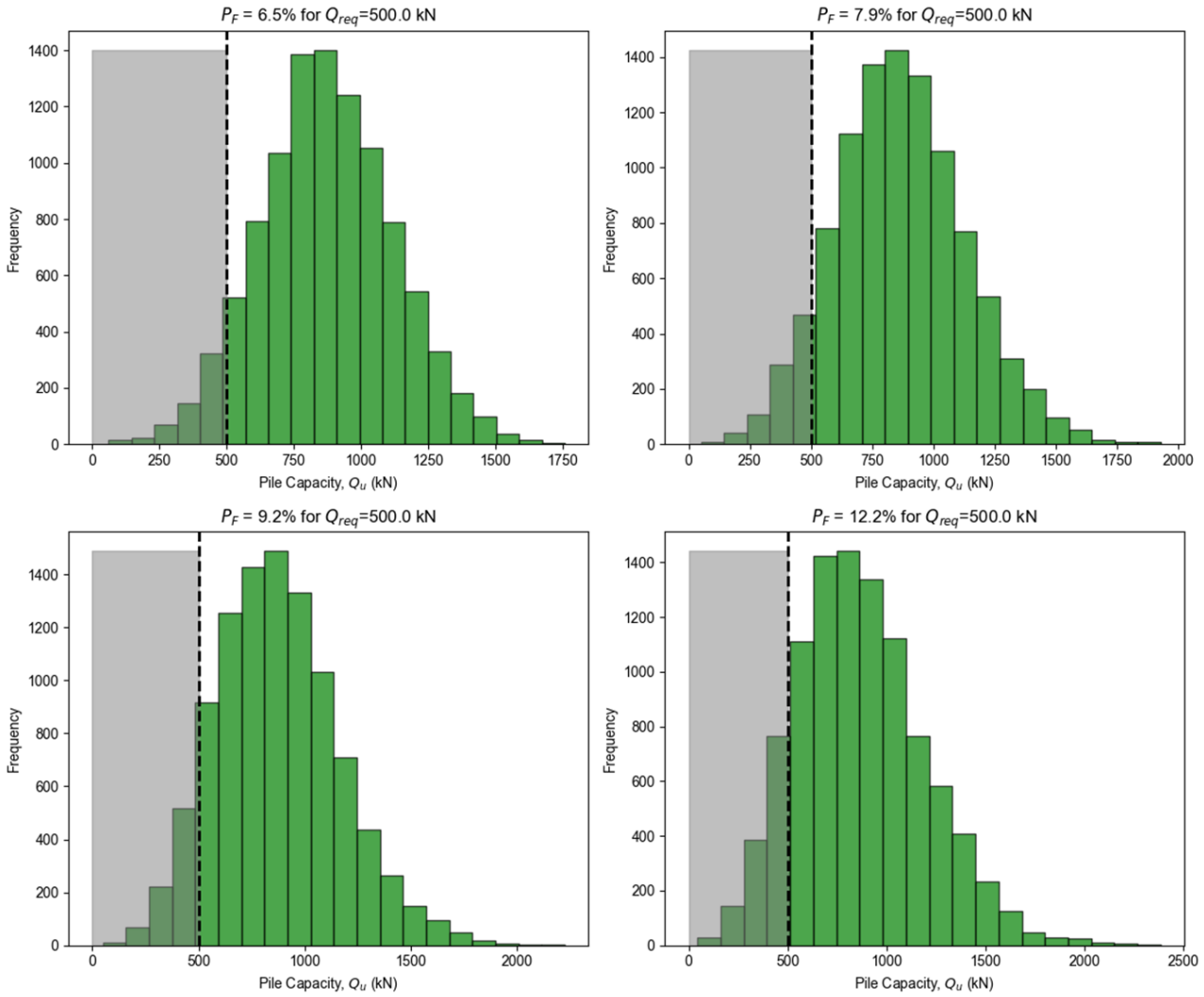

Figure 22: Probabilistic axial capacity distribution for different active layer thickness distributions. Top row from left to right: $L_a = 2.5\ m \pm 0.4\ m$ and $L_a = 2.5\ m \pm 0.8\ m$. Bottom row from left to right: $L_a = 2.5\ m \pm 1.2\ m$ and $L_a = 2.5\ m \pm 1.6\ m$ The permafrost temperature distribution considered in all four cases is $T = -3.2\ °C \pm 1.2\ °C$.

4.4.3 Sensitivity to Permafrost Temperature

Similarly, sensitivity analyses are performed with respect to the permafrost temperature. Keeping a similar mean permafrost temperature of -3.2 °C, we consider four different standard deviations: 0.5 °C, 1.0 °C, 1.5 °C and 2.0 °C. In all four cases, the mean and standard deviation values for the active layer thickness are kept as 2.5 m and 1.0 m, respectively.

Figure 23 show the axial pile capacity distribution results obtained for the four cases. The two plots in the top row show the results for permafrost temperature distributions of T = -3.2 °C ± 0.5 °C and T = -3.2 °C ± 1.0 °C and those in the bottom row show the results for T = -3.2 °C ± 1.5 °C and T = -3.2 °C ± 2.0 °C. The failure probabilities are found to be 6.9%, 18.6%, 25.8% and 32.2% for the four different permafrost temperature distributions, respectively with their increasing standard deviation values. As expected, the warmer the permafrost, the less the axial capacity where in this case the failure probabilities show a considerable increase increasing uncertainties in permafrost temperature.

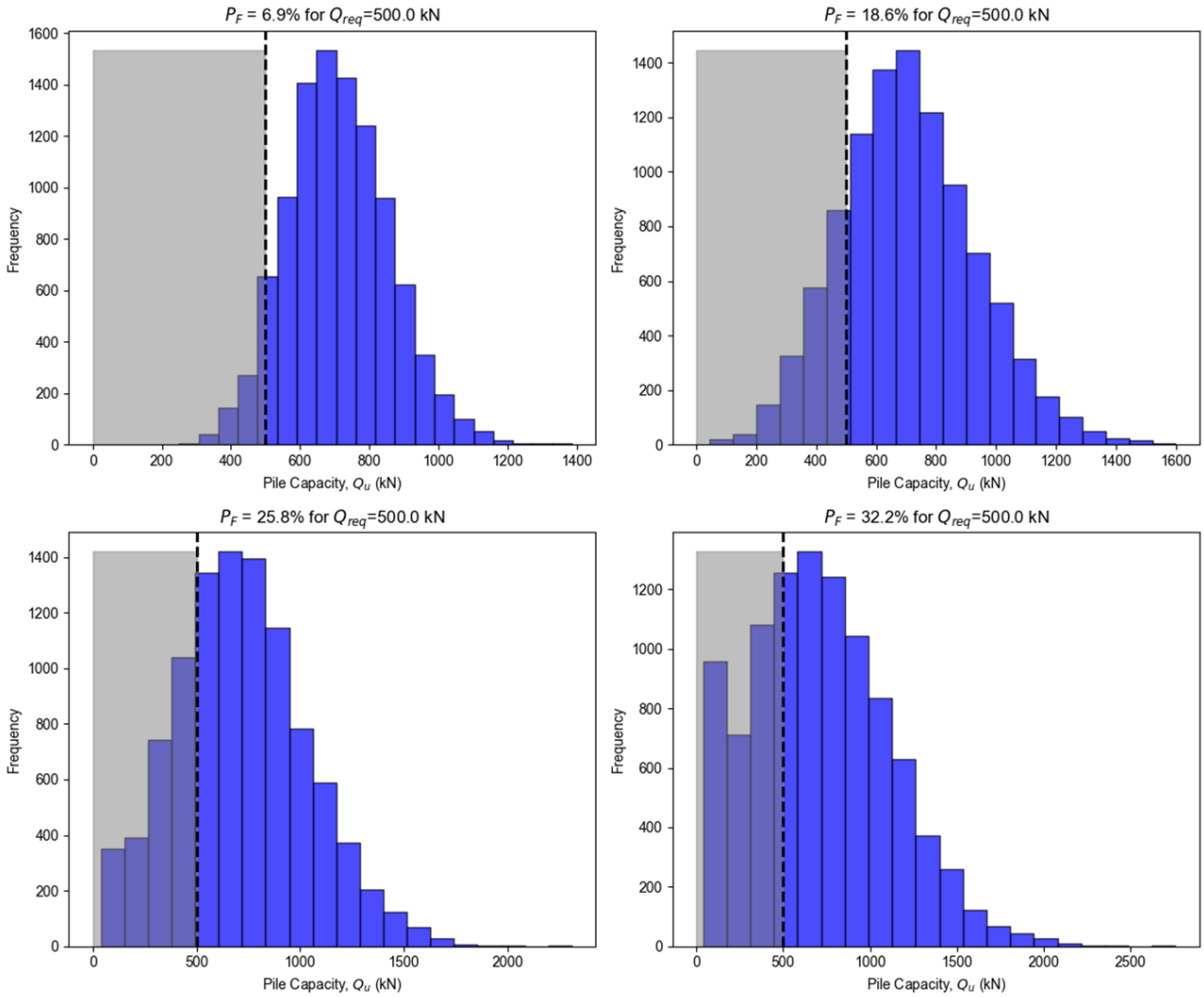

Figure 23: Probabilistic axial capacity distribution for different permafrost temperature distributions. Top row from left to right: $T = -3.2°C \pm 0.5°C$ and $T = -3.2°C \pm 1.0°C$. Bottom row from left to right: $T = -3.2°C \pm 1.5°C$ and $T = -3.2°C \pm 2.0°C$. The active layer thickness distribution considered in all four cases is $L_a = 2.5\ m \pm 1.0\ m$.

5 Conclusions

Based on the ground thermal simulations for the Longyearbyen area, we can draw two significant insights regarding the permafrost characteristics over time.

Firstly, the active layer thickness, which is the top layer of soil that thaws during the summer and freezes again during the winter, is predicted to experience a considerable increase. Over the span of nearly seven decades, from 2001 to the threshold of 2070, the active layer increases in thickness from approximately 1 meter to more than 2 meters. This increase signals a notable shift in ground conditions, which can have profound effects on infrastructure stability, ecosystem dynamics, and carbon release from permafrost areas. However, it is important to note that the projections come with a significant degree of uncertainty, especially in the final decade (2060 – 2070). This uncertainty is attributed to the large standard deviations in the projected temperature data, suggesting that the actual thicknesses could vary widely, with worst-case scenarios predicting the active layer could exceed 3 meters.

Secondly, the permafrost, which is the layer of soil below the active layer that remains frozen year-round, is also undergoing a warming trend. The simulations indicate that the permafrost temperature has been steadily increasing, with a rise from about -4.5°C in 2001 to an anticipated -3.2°C by the end of 2070. Although there is some uncertainty associated with these temperature projections, it is relatively smaller when compared to the uncertainties in the active layer thickness predictions. The increase in permafrost temperature is a concerning indicator of climate change effects in polar regions, as it can lead to the thawing of permafrost and the consequent release of greenhouse gases, along with potential damage to infrastructure designed for colder conditions.

A probabilistic analysis methodology for evaluating the axial capacity of piles in permafrost conditions is developed, showcasing the nuanced approach that accounts for uncertainties in environmental and material properties, which traditional deterministic models may overlook. This methodology, exemplified through Monte Carlo simulations, incorporates variability in critical parameters such as the active layer thickness and permafrost temperature, delivering a spectrum of possible outcomes rather than a singular, fixed-value result. This approach provides a deeper insight into the structural performance and risk profiles under diverse scenarios, emphasizing the importance of acknowledging and integrating such uncertainties into the geotechnical design and assessment processes to enhance the reliability and safety of the structures.

Further, the sensitivity analyses conducted as part of the methodology highlight the significant influence of probabilistic parameters on the failure probabilities of the piles. By adjusting the standard deviations of the active layer thickness and permafrost temperature, the analyses reveal how these uncertainties can markedly affect the structural capacity and, consequently, the failure risk. This aspect of the probabilistic analysis underpins the critical role of considering variable factors in structural capacity assessment, aiding in the identification of key influencers on structural performance. It advocates for a probabilistic approach in geotechnical engineering, offering a more dynamic, adaptable framework for decision-making under uncertainty compared to the more rigid deterministic models, thus promoting better risk management and design optimization in challenging permafrost environments.

References

Andersland, O.B., Ladanyi, B., 2003. Frozen Ground Engineering. John Wiley & Sons.

Bekele, Y., Sinitsyn, A., 2023. Risk Analysis of the Impact of Natural Hazards on Cultural Heritage: Development of a Risk Assessment Tool (No. 2023:00250).

Christiansen, H.H., Gilbert, G.L., Demidov, N., Guglielmin, M., Isaksen, K., Osuch, M., Boike, J., 2019. Permafrost thermal snapshot and active-layer thickness in Svalbard 2016-2017. Svalbard Integrated Arctic Earth Observing System, Longyearbyen. https://doi.org/10.5281/zenodo.4777825

Gilbert, G.L., Instanes, A., Sinitsyn, A.O., Aalberg, A., Gilbert, G.L., Instanes, A., Sinitsyn, A.O., Aalberg, A., 2019. Characterization of two sites for geotechnical testing in permafrost: Longyearbyen, Svalbard. AIMS Geosci. 5, 868–885. https://doi.org/10.3934/geosci.2019.4.868

Landgren, O., Lutz, J., Isaksen, K., 2025. 2.5 km future climate projections for Svalbard under the high emission scenario SSP5-8.5 (No. MET Report 1/2025).

Tsegaye, A.B., Guegan, E. Nordal, S., 2015. Modeling the strength of frozen saturated soil. Norwegian University of Science and Technology, Trondheim, Norway.

Weaver, J.S., Morgenstern, N.R., 1981. Pile design in permafrost. Can. Geotech. J. 18, 357–370. https://doi.org/10.1139/t81-043